

CARMA Memorandum Series #36

CARMA Holography

Stuartt Corder & Melvyn Wright

^a: *Division of Physics, Mathematics & Astronomy, California Institute of Technology, Pasadena, CA, 91125*; ^b: *Radio Astronomy laboratory, University of California, Berkeley, CA, 94720*

October 19, 2006

ABSTRACT

We obtained low resolution holography of the 15 antennas of the Combined Array for Research in Millimeter Astronomy (CARMA) to determine the primary beam voltage patterns, antenna illumination patterns and large scale surface errors. The strong, unresolved source 3c273 was used to measure the voltage patterns of the six 10.4 m antennas using the nine 6.1 m antennas as reference antennas and vice versa. We obtain a resolution of $27''$ and $46''$ on the sky for 10 m and 6 m antennas, respectively. These give amplitude and phase in the aperture plane with a resolution of 0.71 m for 10 m antennas and 0.42 m for 6 m antennas. The holography measurements showed that the dominant error for the 10 m antennas was an offset in the antenna illumination pattern. These errors were corrected using optical alignment. For the 6 m antennas, the dominant error was large surface deviations which were directly measured from the holography, and were corrected by mechanical adjustments of the panels.

Change Record

Revision	Date	Author	Sections/Pages Affected
			Remarks
1.0	2006-May-18	SAC	1-6
	Draft memo		
1.1	2006-Aug-08	SAC	1-6
	revision		
1.2	2006-Sep-06	SAC	1-6
	revision		
1.2	2006-Sep-19	MCHW	1-23
	revision		
1.2	2006-Oct-19	MCHW	1-23
	revision		

1. Introduction

The Combined Array for Research in Millimeter Astronomy (CARMA) is currently composed of six 10.4 m (C1–C6) and nine 6.1 m (C7–C15) antennas. In transportation to their current location at Cedar Flat, the antennas were subjected to a range of stresses that they had previously not experienced. Therefore, it is important to verify the optical and receiver alignment, and the antenna illumination and surface shape of these antennas. Deviations in illumination pattern and large scale surface errors result in poorer than expected signal to noise and incorrect primary beam deconvolution from mosaiced images.

To measure deviations from the ideal illumination and shape of the primary beam, we must measure the shape of the voltage pattern on the sky. Fourier transforming the amplitude and phase voltage pattern provides an image of the amplitude and phase pattern in the aperture plane. When convolved by the low resolution holography the expected amplitude of the aperture illumination is a ring with a depression in the center due to subreflector blockage and a Gaussian taper toward the edges. Feed legs blockage prevent this ideal pattern from being seen in high resolution maps, but the general pattern should be as symmetric as possible. The phase across the aperture should be constant.

Deviations in the aperture illumination can be caused by misalignment of the optics of the antenna or receiver. Deviations in the aperture phase pattern can be caused by antenna pointing errors, resulting in linear gradients, and focus errors, resulting in quadratic terms. These effects can be corrected by peak-up pointing and antenna focus adjustments. Higher order deviations indicate problems with the antenna surface that must be removed by other means. These higher order terms can be caused by stresses imposed by the panel backup structure. Both large scale and localized deformations may be present though higher resolution than that discussed here is necessary to determine localized deformations.

2. Data Collection

Holographic data of the 15 Carma antennas were obtained using the bright, unresolved source 3c273 at a frequency of 88.5 GHz (3.4 mm). To determine the primary beam voltage patterns, antenna illumination and large scale surface errors, the 6 m antennas tracked the source as reference antennas while the 10 m antennas were stepped through a square, 19 by 19 pointing grid at 80% of the Nyquist step size at the LO frequency. Points beyond a radius of 9 grid points were skipped, resulting in a circular beam pattern. To facilitate self calibration, the center position was observed at the beginning of each row of the scan, and, when applicable, every seventh observed point within a row. An additional center pointing was observed at the completion of the pointing grid. The antenna sets were then switched with 10 m antennas serving as reference for the 6 m antenna voltage pattern measurements. The step size was adjusted accordingly. Final maps afforded a resolution of 27'' and 46'' on the sky for 10 m and 6 m antennas, respectively.

Given the constant upgrade and testing of the antennas at Cedar Flat, the holography datasets never included all 15 antennas. We therefore rely on a compilation of datasets which cover all antennas. Because of this, the number of reference antennas available for verification of repeatability differs from dataset to dataset. Typically, each 10 m antenna had 5 to 6 reference antennas and each 6 m antenna had 3 to 4 reference antennas. Also, uniform data quality is not possible because some antennas were not available on days with the best observing conditions.

3. Data Reduction & Analysis

Calibration and holographic imaging of the antenna surface was made using MIRIAD (Sault, Teuben, & Wright, 1995). The dataset was split into separate 500MHz frequency bands for both LO sidebands. Self calibration was performed on the separate windows. In order to calibrate, we required a method to separate the central pointings. This was done by replacing the u and v coordinates with delta azimuth and delta elevation. The central pointings were then used to calibrate the data by selecting $(DAZ, DEL) = (0,0)$ by using MIRIAD's `select=uvnrange`. For each antenna, the resulting calibrated voltage patterns for each reference antenna and frequency band were converted to real and imaginary parts, Fourier transformed from the sky plane to the aperture plane using the MIRIAD `fft` function, and masked to exclude any information arising from outside the aperture. These observations result in amplitude and phase in the aperture plane with a resolution of 0.71 m and 0.42 m for 10 m and 6 m antennas, respectively.

The individual apertures images were then fit using the MIRIAD task `imhol`. `Imhol` fits a function to the aperture phase accounting for the size of the secondary, removes principal-axis focus and pointing errors, and provides a new image data set with these errors removed. `Imhol` also calculates an RMS surface error, in microns, both before and after the phase function fit, as well as an illumination weighted post-fit RMS surface error. The pointing and focus error subtracted images and fits were examined to verify that the solutions and residuals were consistent across frequency bands, upper and lower sideband of the LO, and reference antennas. A single, average image was then created. This averaging was done in the aperture plane to minimize the effects of the differing frequencies in each band.

To determine the orientation of the resulting images a piece of Mylar was placed on one 6 m and one 10 m antenna. The Mylar, possessing an index of refraction greater than 1, induces a phase lag for incident radiation. In the aperture plane, this appears as a depression in the antenna surface. The Mylar was placed on a 6 m antenna and was discovered in a blind test of our reduction process, establishing the orientation of the 6 m antenna images. For the 6 m antennas the aperture images need to be flipped top to bottom. Similar tests performed on 10 m antennas were more difficult given the physical resolution was poorer on the 10 m antennas. For the 10 m antennas the baseline order is reversed and the signs are expected to be reversed. The Mylar induces a raised antenna surface implying that the sign of phase was indeed reversed. However, further tests with higher resolution are required for verification.

For high image fidelity, especially for mosaicing, the RMS surface error of the antennas, after the removal of pointing and focus errors, should be $\sim 1/40$ of the observing wavelength (Cornwell, Holdaway & Uson, 1993). Therefore, a target of 30 μm RMS surface accuracy is desired for 1.3 mm observations. The 30 μm RMS is referred to as the benchmark in what follows.

4. Results

4.1. Figure Layout & General Properties

Figures 1-15 display the amplitude and phase patterns both before (left panel) and after (right panel) adjustment except where no adjustment was done. In cases without adjustment, the two panels serve to indicate repeatability of measurement. Antennas which underwent no adjustment are 1, 2, 3 (one date only), 5, and 9. The figure axes are in wavelength units and each figure consists of a color image with black contours. Figure number corresponds to Carma antenna number. Figures are orientated as described in the text implying, for example, that the 6 m antenna images need to be flipped top to bottom.

The illumination pattern, shown in color, is provided to give information about the optical alignment of the system. The region of depressed illumination near the center is the shadow of the secondary. The illumination pattern also serves as a weighting function for surface errors; regions with large surface errors may not significantly impact antenna performance if those regions are associated with low illumination.

The phase residuals, i.e. post pointing and focus correction, are shown as contours and are expressed as surface errors. Negative contours (dashed) are at -25, -50, -75 and -100 μm surface deviations. Positive, solid contours are at 25, 50, 75 and 100 μm surface deviations. Table 1 displays the summary of surface errors. Antennas for which no panel adjustment was made have a single value for RMS surface error.

4.1.1. *Carma 1*

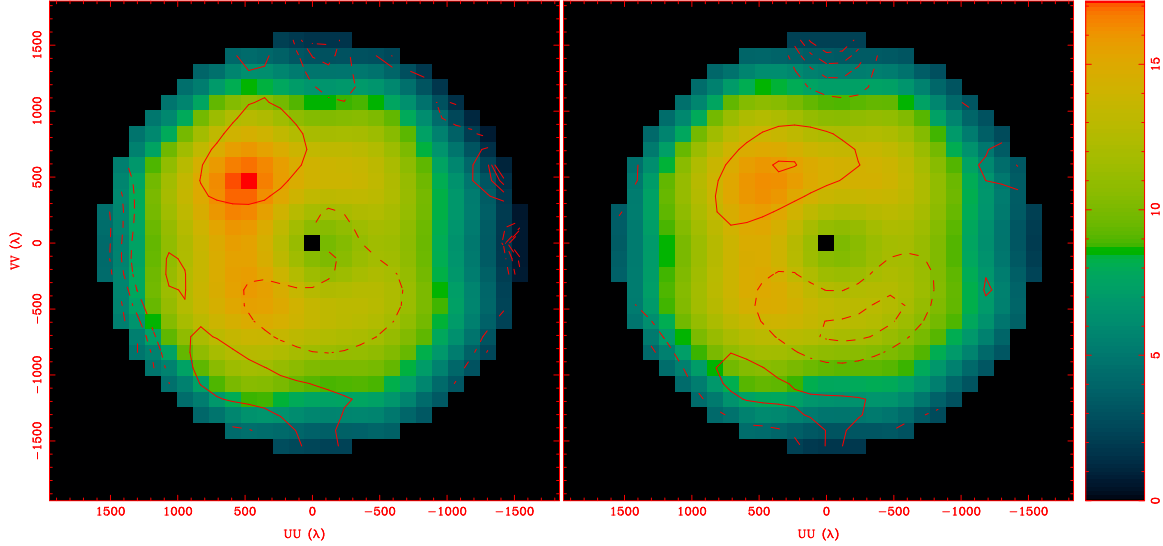


Fig. 1.— These data were obtained 2006 June 12 and 22. The illumination pattern is reasonably well centered and did not require alignment. Panel adjustments were not done on this antenna. This allows a display of our repeatability (left: June 12, right: June 22). We find 25-50 μm errors consistently in the same places on each image, e.g. at the top, the upper-left of center, lower-right of center, and bottom of the image, indicating that we could do correction at that level. Despite being in a region of poor illumination, the top of the image consistently shows strong negative phase, indicating a correction here may be useful. The RMS surface error is 25 μm , better than the benchmark, with a slight, 2-3 μm degradation if we do not weight by the illumination pattern.

4.1.2. *Carma 2*

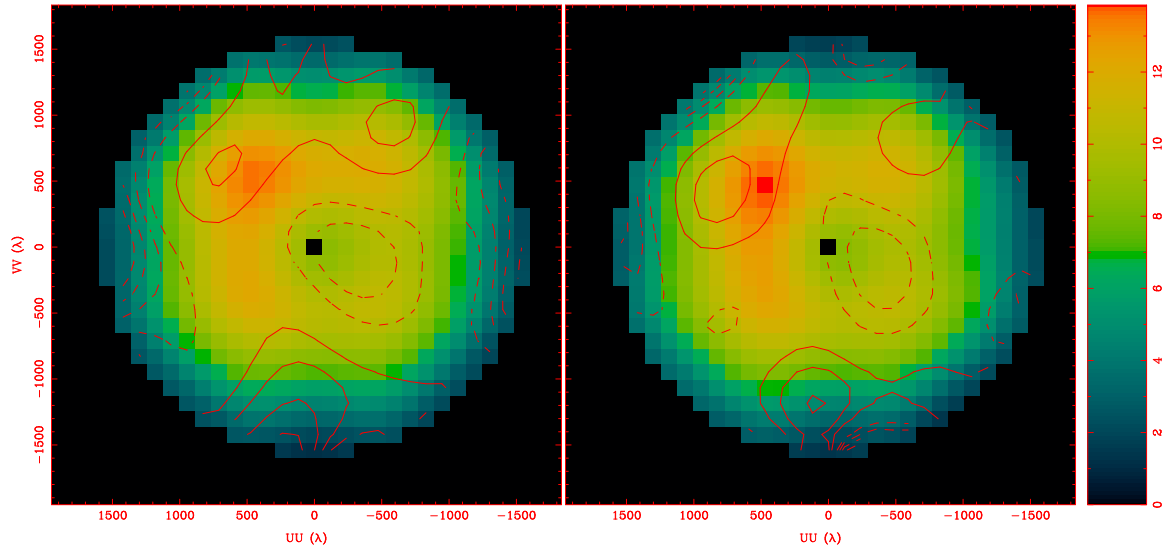


Fig. 2.— These data were obtained 2006 May 10 and June 12. The illumination pattern is offset slightly towards the top of the image but it is unclear if alignment will provide benefit given the amount of improvement seen in multiple attempts of re-alignment on other more deviant antennas (see Carma 4). The phase pattern is marginally astigmatic, with 2-fold symmetry seen. As with C1, no alignment or adjustment was done. There are two relatively centered 50 μm surface errors, one up towards the top left, near the peak of the illumination pattern and one right of center. The bulk of the antenna phase errors are displaced towards the outer edge, an effect echoed in the surface RMS which increases from 37 μm to 45 μm when weighting by illumination pattern is omitted. Modest panel adjustments seem to be required here but the antenna is not far from the 30 μm RMS benchmark.

4.1.3. *Carma 3*

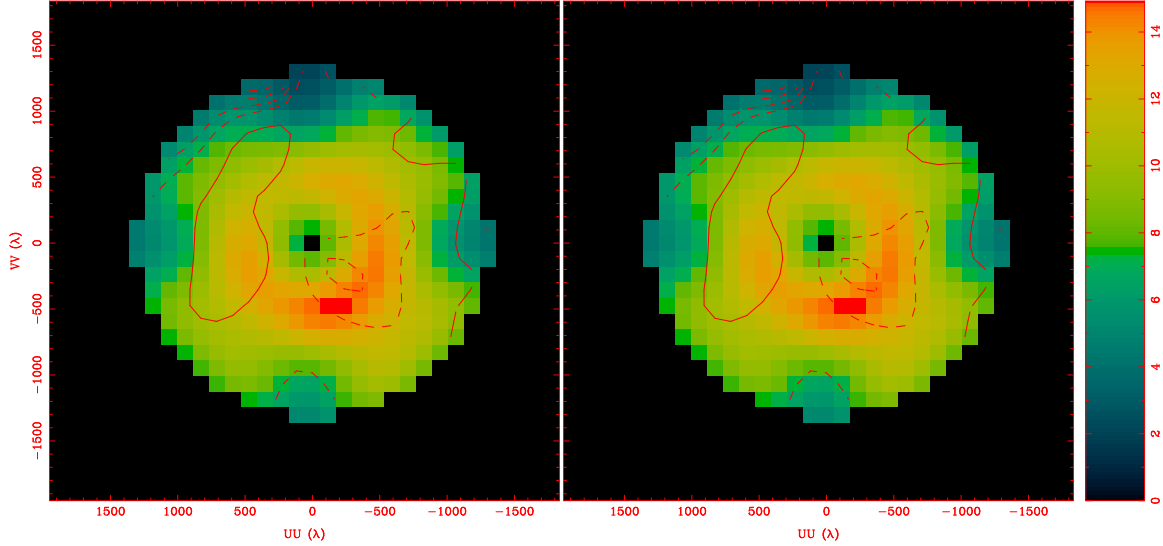


Fig. 3.— Due to receiver work, this antenna has only one data set obtained 2006 April 25, earlier than the other antennas and with poorer resolution. The data is displayed twice simply to maintain consistency with other figures. The illumination pattern appears highly quadrupolar mostly due to data collection methods that were changed in later datasets. In general, though, the illumination pattern is reasonably well centered with perhaps a slight displacement towards the bottom of the figure. The phases are particularly good on this antenna with only the top right of the figure, a region with poor illumination, being largely deviant. The RMS surface error here is 30 μm , i.e. at benchmark, with 2-3 μm degradation when not weighting by the illumination pattern. A more recent dataset with standard data collection will be requested when C3 becomes available again for observing.

4.1.4. *Carma 4*

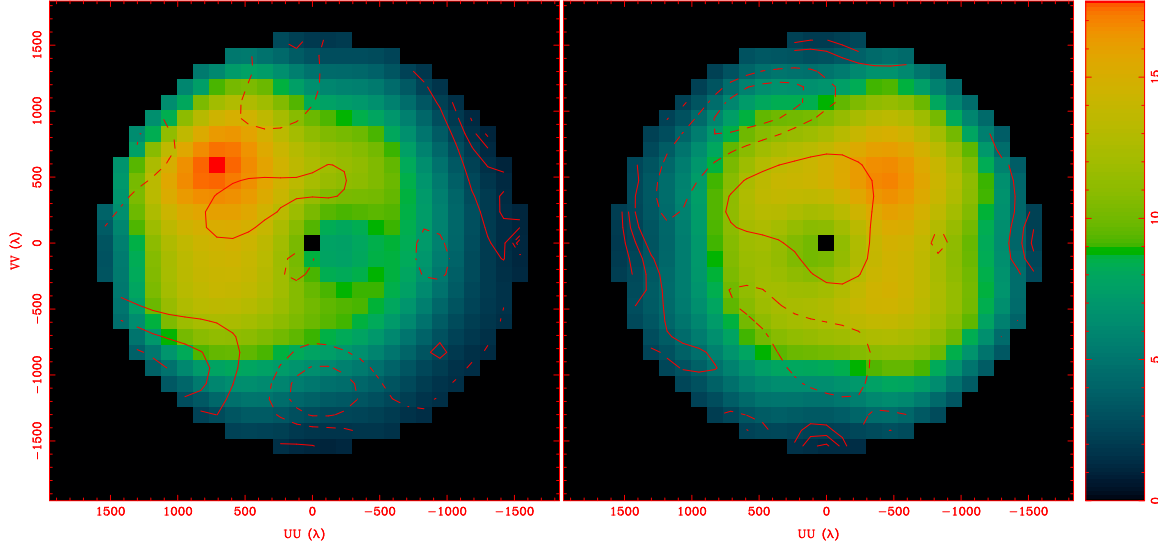


Fig. 4.— These data were obtained 2006 May 10 and June 12. The illumination pattern is not well centered in the pre-alignment image. Judging by the distance from the peak to the antenna center, we had a 2.8 m offset. After being re-aligned twice, the emission is clearly more centered on the antenna surface. While difficult to estimate, the residual error is likely less than 0.5 m. No panel adjustments were made on this antenna. The later data with a more centered illumination pattern should more accurately represent the true surface error. The post-alignment surface RMS is 28 μm , less than the benchmark value, with only slightly poorer value when the illumination weighting is not included.

4.1.5. *Carma 5*

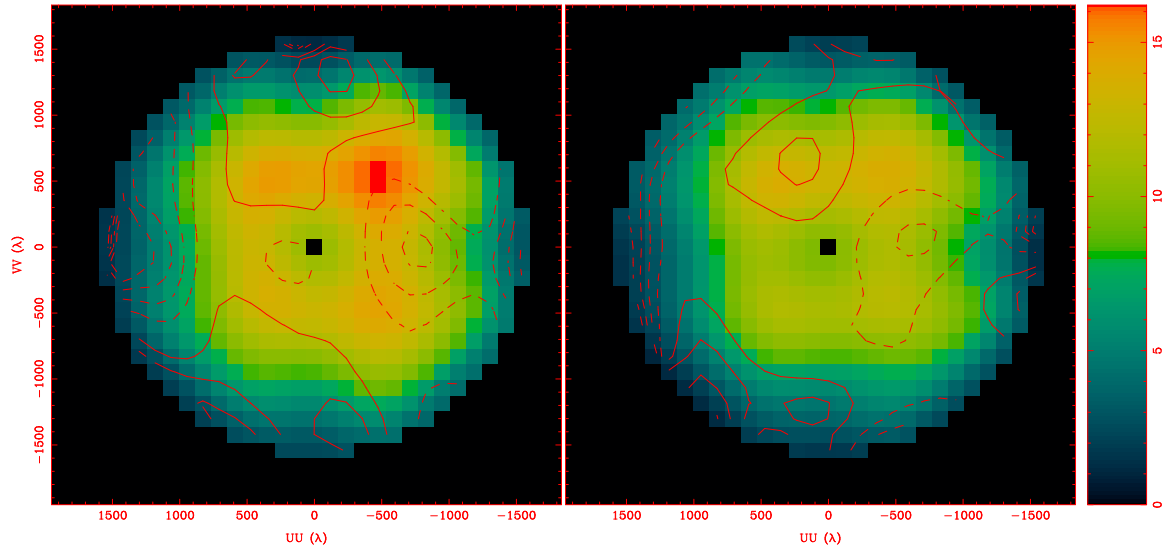


Fig. 5.— These data were obtained 2006 May 10 and 30. The illumination pattern is slightly offset to the top right of the image but not enough to require alignment. No panel adjustment was done on this antenna. The surface errors are large near the antenna edges, particularly on the top and right of the figure. One region right of center seems consistently negative and could be adjusted. The surface RMS is 33 μm when weighted by illumination pattern and 39 μm when not weighted. Minor adjustment would allow this antenna to meet the benchmark.

4.1.6. *Carma 6*

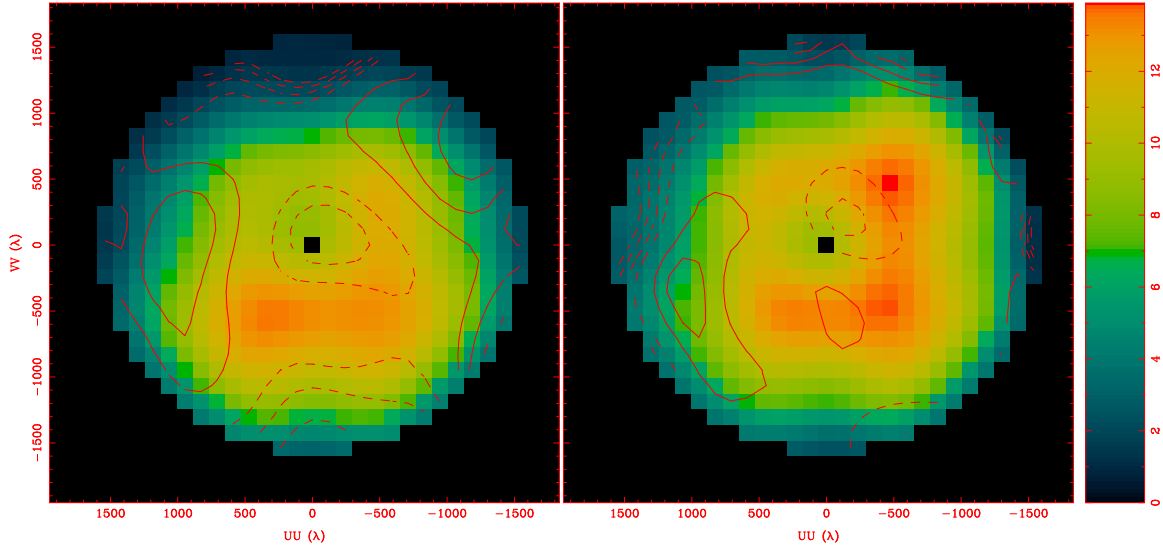


Fig. 6.— These data were obtained 2006 May 10 and June 12. The alignment was adjusted between these datasets. The later dataset shows a more symmetric profile and appears to require no further adjustment. There is a negative phase error slightly right of center in the map. The region to the left appears consistently positive. These particular regions may benefit from panel adjustment. Other regions of significant deviation are in regions of poor illumination which is evidenced by the growth of the surface RMS from 30 μm to 40 μm when the illumination pattern weighting is ignored. Adjustment may bring much better surface RMS than the already achieved benchmark.

4.1.7. *Carma 7*

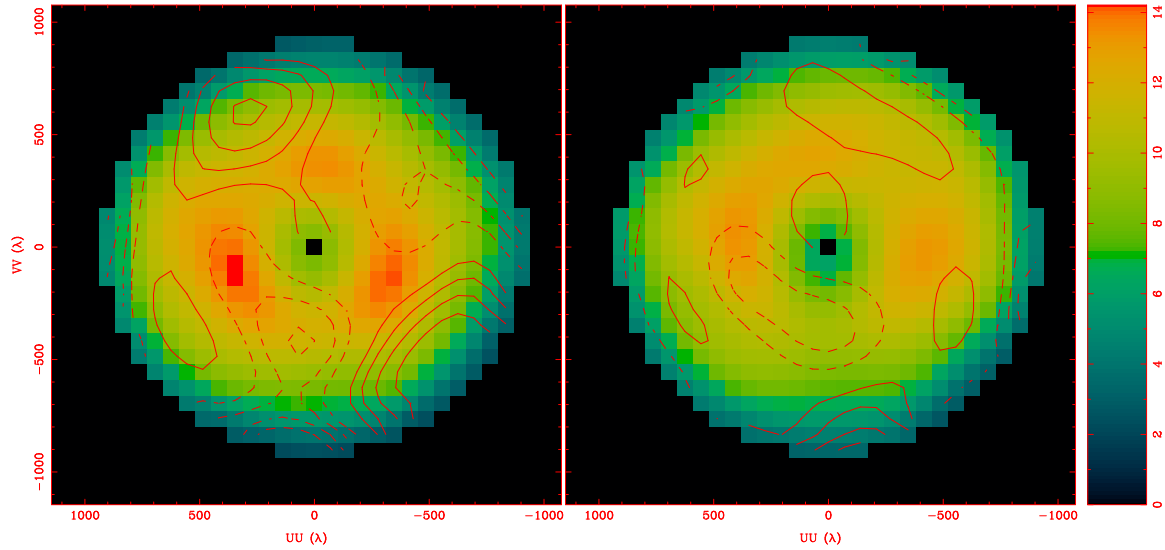


Fig. 7.— These data were obtained 2006 May 30 and June 22. On the left, the illumination pattern is well centered and merits no further comment. The RMS surface accuracy is 50 μm , or 60 μm if illumination weighting is not included. The significant residual surface error appears to have a three-fold symmetry with three sets of positive surface error and three of negative surface errors. Post adjustment, the surface RMS is ~ 30 μm with little dependence on the illumination pattern. This antenna is now at the benchmark for surface accuracy.

4.1.8. *Carma 8*

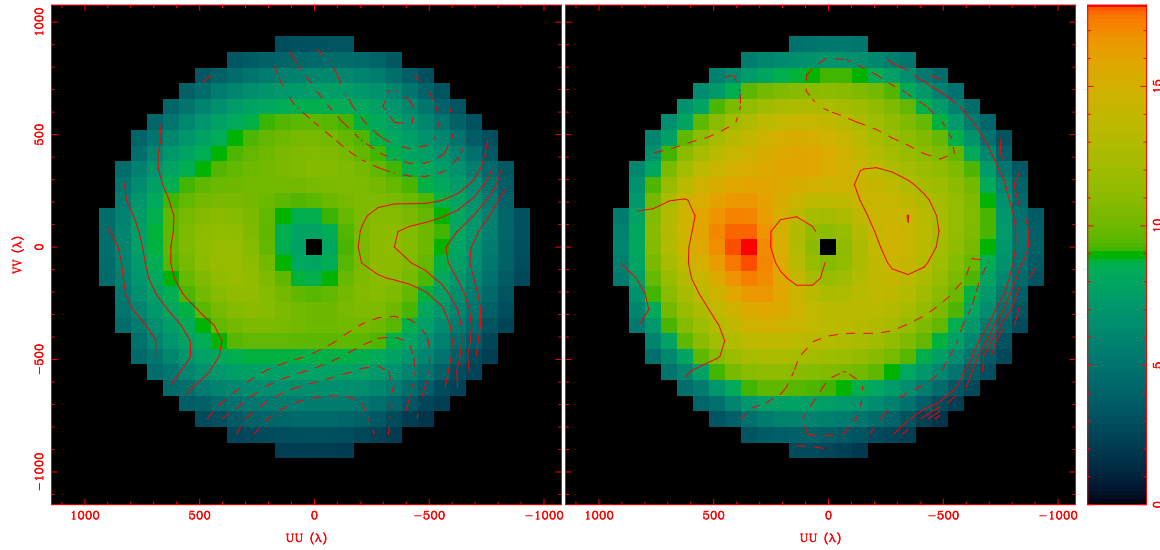


Fig. 8.— These data were obtained 2006 May 30th and June 22. The illumination pattern is slightly off center, towards the top left, but the error is not very significant. The pre-adjustment RMS surface error is about 50 μm (55 μm if not weighted by the illumination pattern). The pattern here appears to have a two fold symmetry, classic astigmatism. Post adjustment, the antenna has 30 μm surface RMS but with still some dependence on the illumination pattern. This antenna is now at the benchmark for surface accuracy.

4.1.9. *Carma 9*

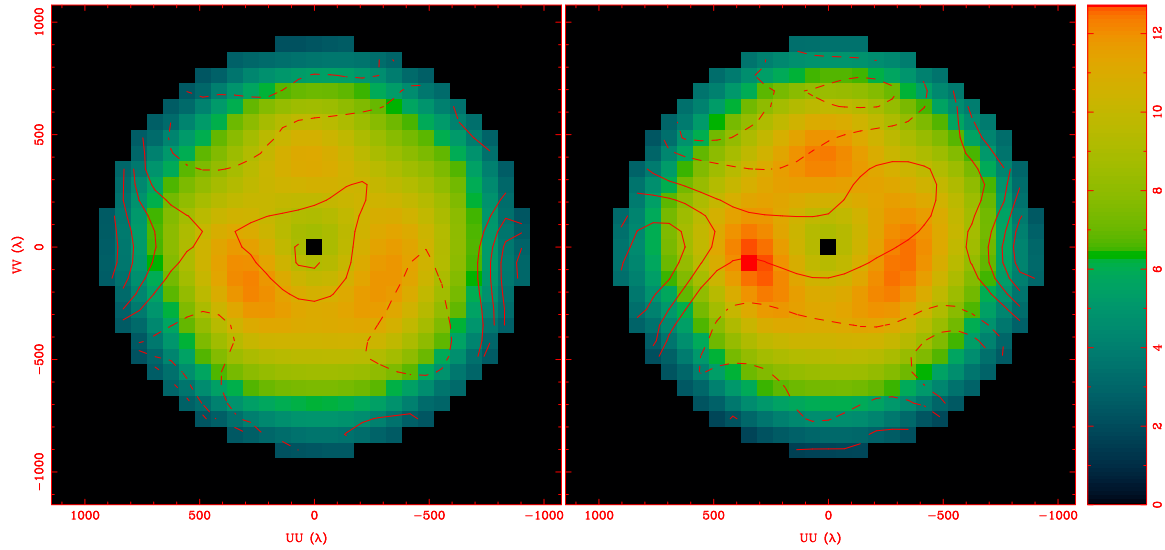


Fig. 9.— These data were obtained 2006 June 12 and 22. The illumination pattern is well centered. This antenna was not adjusted. The RMS surface accuracy is ~ 35 μm with another 5 μm added if illumination weighting is not included. There is a hint of the 3-fold symmetry here but given the lack of significant surface error in the middle of the antenna we await higher resolution before adjusting this surface.

4.1.10. *Carma 10*

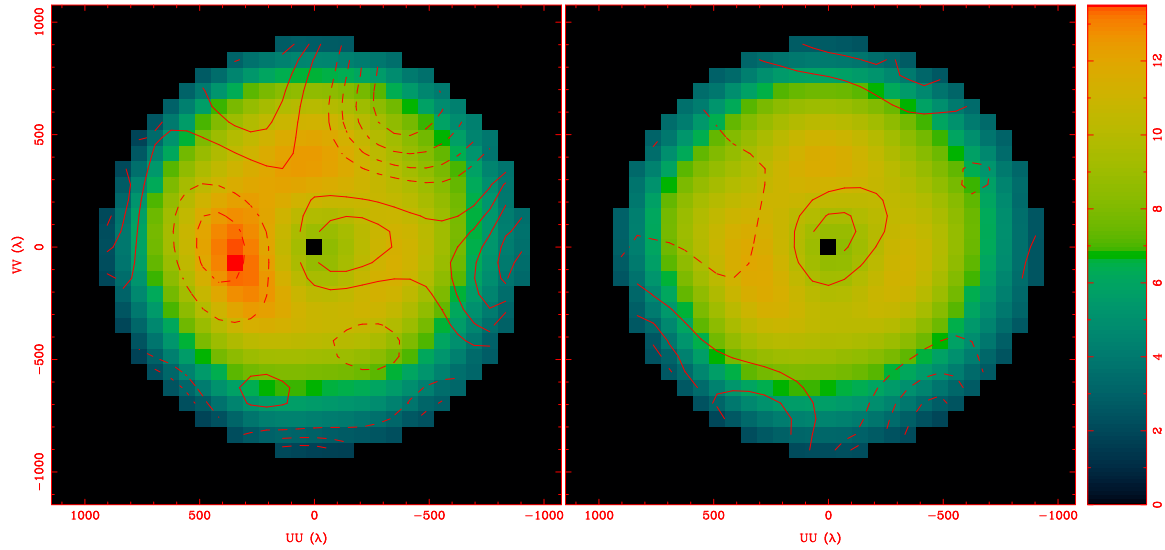


Fig. 10.— These data were obtained 2006 May 10 and June 12. Here the illumination pattern is offset towards the top, however adjustment of the alignment on the 6 m antennas is difficult and the error is not likely significant enough to address at this time. The 2-fold symmetry appears in the pre-adjustment data and is still visible post adjustment. The RMS surface accuracy prior to adjustment is 40 μm when weighted by the illumination pattern. Post adjustment the surface RMS is reduced to 32 μm or 38 μm without illumination weighting indicating a residual dependence on illumination pattern. This antenna is nearly at the surface accuracy benchmark.

4.1.11. *Carma 11*

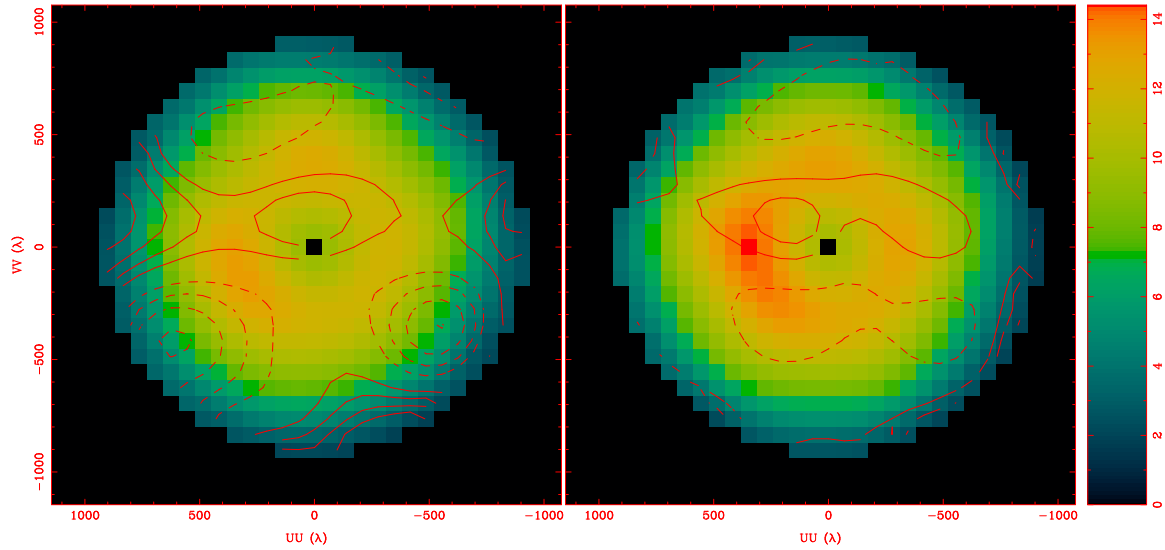


Fig. 11.— These data were obtained 2006 May 23 and June 22. The illumination pattern is well centered. There is some indication of 3-fold symmetry in the pre-adjustment data. In that map, the surface RMS is 42 μm using illumination pattern weighting, without weighting the RMS is nearer 50 μm . Post adjustment, there is little remaining structure with surface RMS now independent of illumination pattern and has a value of ~ 30 μm which is at the surface accuracy benchmark.

4.1.12. *Carma 12*

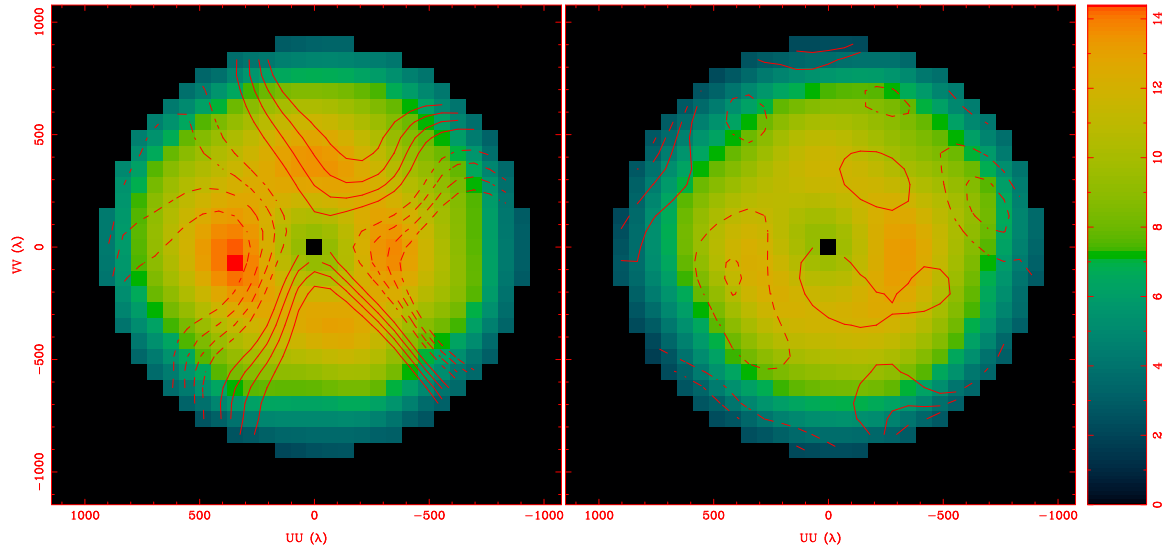


Fig. 12.— These data were obtained 2006 May 30 and June 12. The illumination is well centered. Prior to adjustment, we find very strong signatures of astigmatism. The RMS surface error is 110 μm when weighted by the illumination pattern, not including weighting brings the RMS to 130 μm . Post adjustment, we have reduced the surface error to 29 μm for the illumination weighted value with only modest dependence on illumination pattern. This antenna is now at the surface accuracy benchmark.

4.1.13. *Carma 13*

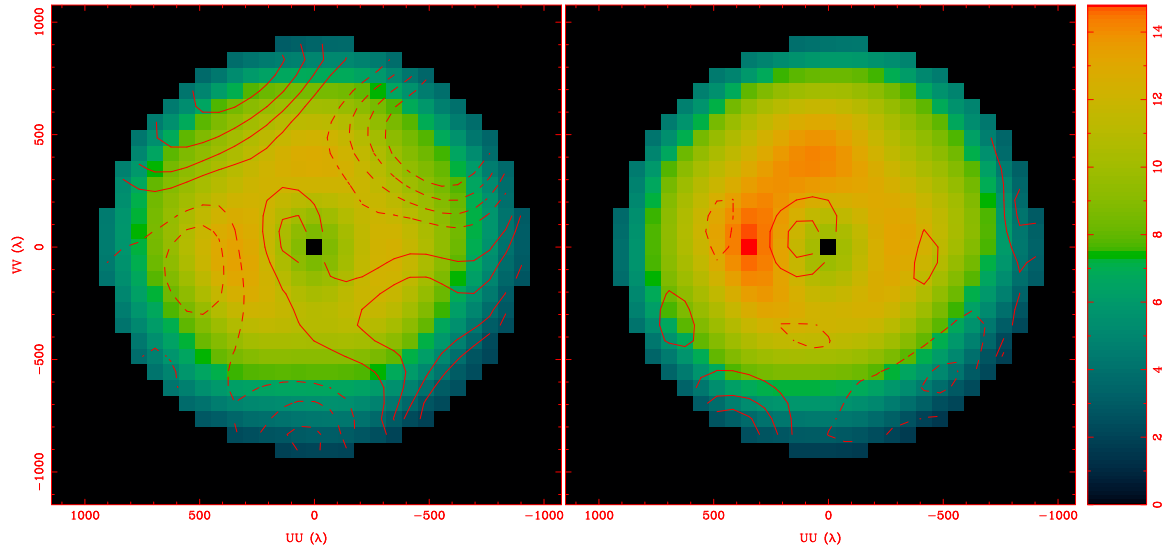


Fig. 13.— These data were obtained 2006 May 30 and June 22. The illumination pattern is slightly offset to the top left but the offset is not severe. Pre-adjustment there is a strong astigmatic signature with illumination weighted surface RMS of 55 μm . Post adjustment there is little to no signature left, with surface RMS now 23 μm and mostly independent of illumination pattern. This antenna has surpassed the surface accuracy benchmark.

4.1.14. *Carma 14*

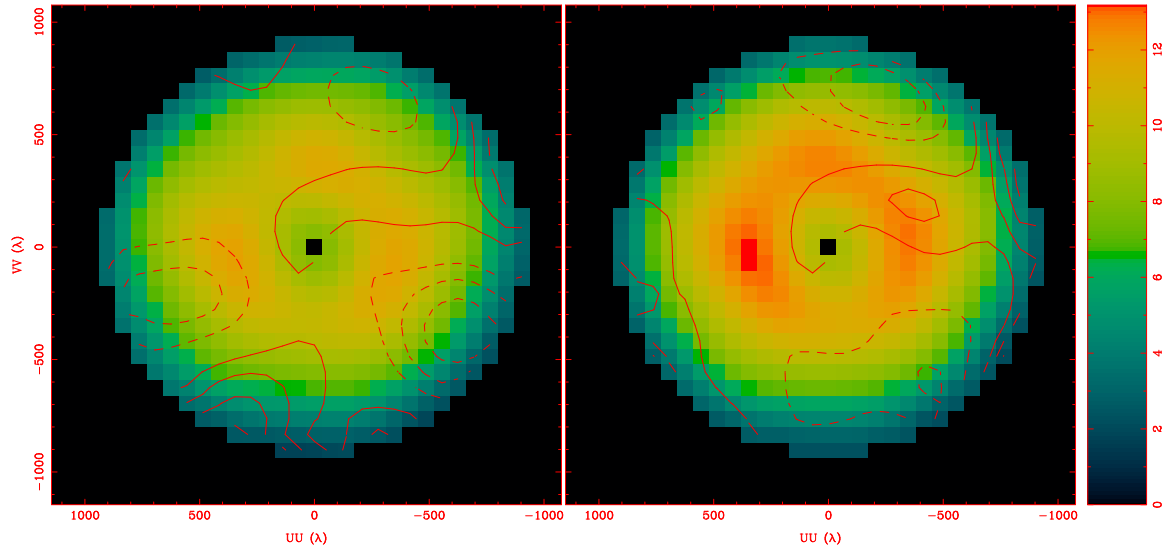


Fig. 14.— These data were obtained 2006 May 30 and June 22. The illumination pattern is well centered. Pre-adjustment we see an RMS surface error of 34 μm when weighting by the illumination pattern while the post adjustment value is 29 μm with only slight dependence in illumination. Pre-adjustment we see signs of 3-fold symmetry which are not evident post adjustment. This antenna is now at the surface accuracy benchmark despite there being signs on the right side of the image that further improvement could be made.

4.1.15. *Carma 15*

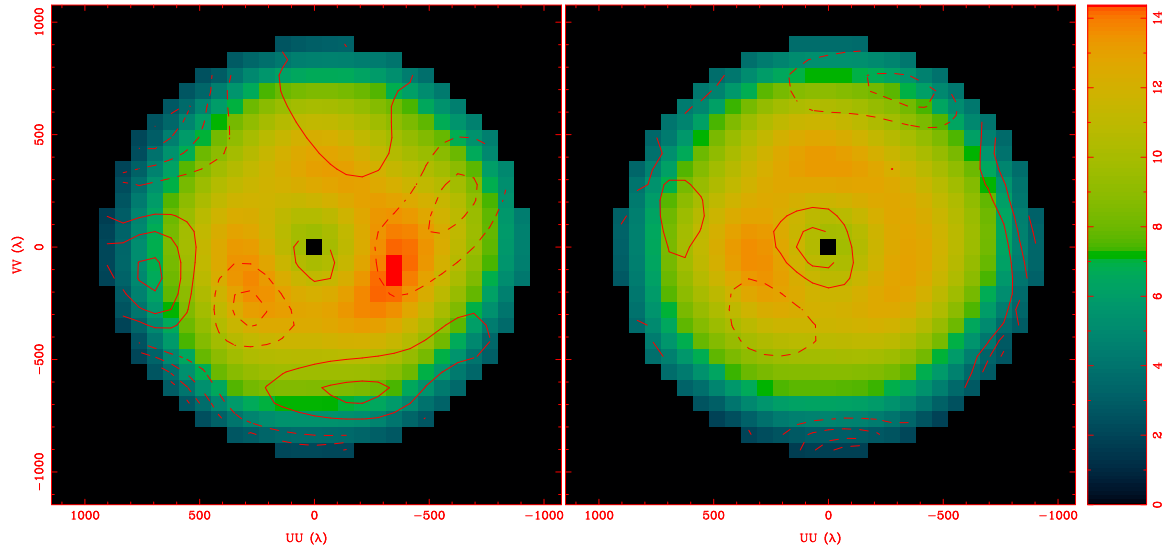


Fig. 15.— These data were obtained 2006 May 10 and June 22. Again, the illumination pattern is well centered. Prior to adjustment, we see signs again of the 3-fold symmetry. Illumination weighted RMS surface errors are 33 μm . Post adjustment, the RMS surface error is down to 25 μm though still marginally dependent on illumination pattern. This antenna is better than the surface accuracy benchmark.

4.2. Antenna Summary

Prior to an alignment campaign, the most significant optical alignment error, on C4, resulted in an illumination pattern offset by 2.8 m. After realignment of the optical path on C4 (twice) and C6 (once) via a laser shimming tool designed to make small corrections to the mirror alignment, the 10 m antennas all have comparable illumination offsets. Further alignment of the 10 m antennas is available only at considerable cost in time. It is unclear that any significant gain would be made. Illumination alignment of the 6 m antennas is not significantly offset in any antenna. The optical path is simple and viable locations for adjustment are not available.

Adjustment of 10 m surface panels is marginally necessary in two cases, C2 and C5. Small gains to the already acceptable surface accuracy of the other 10 m antennas appear to be possible. Before panel adjustment on the 6 m antennas, significant deviations existed on nearly all antennas. Only C9 was deemed good enough to not adjust. C12 showed the most problematic surface, with sections of the antenna surface showing over 300 μm deviations. Therefore, we used C12 as our test case for the adjustment procedure. Figure 12 (left panel) was smoothed to approximately centimeter resolution to provide sub-panel information. Given the 1 mm per turn pitch of the mounting screws, we converted the micron offsets to degrees of screw turn. The four screws at the corners of each panel intersection were then adjusted equally.

Adjustments were made in 5 degree increments, beginning at 5 degrees, though later antennas were altered only if the deviation was at least 20 degrees given the repeatability in the holography maps. Adjustments were performed using a two pronged tool that fits directly into the front of the mounting screws. The tool has a protractor mounted on the top to allow accurate adjustment. Given the success demonstrated in Figure 12, we eventually adjusted eight of the nine 6 m antennas to achieve the 30 μm RMS goal.

It is not surprising that the alignment of the 10 m antennas was effected more than the antenna surface. The 10 m optical path is complex. There are many reflections that must be aligned to ensure optimal function. The surface was not altered intentionally in any way prior to transport as such alteration was not deemed necessary. This was not the case for the 6 m antennas. The dish and backup structure were removed from the mounting ring on the antenna and transported separately. When the dishes were lifted back into place at Cedar Flat, gaps of a few millimeters were observed between the mounting rings on the dishes and antenna. The gaps were closed in bolting the dish to the antenna. It is therefore not surprising that there were bulk deformations of the surface with either 2 or 3 fold symmetry as forcing one part of the antenna edge down raised nearby regions and caused a ripple effect. The lowest moment of this deformation would be the classic high-low-high-low signature of astigmatism. The next moment would be the 3-fold symmetry seen on many 6 m antennas.

It also appears that, even post panel adjustment, some 6 m antennas have errors which depend on the antenna illumination pattern. In principal, after adjustment the errors should be uniformly distributed, even if they were not so prior to adjustment. In hindsight this is not surprising as

correction for antenna surface inclination with respect to the vertical was not taken into account. This resulted in an under adjustment increasing towards the outer edge of the dish.

Table 1: RMS surface accuracy of the 15 CARMA antennas in microns. Antennas with single values did not have panels adjusted.

Antenna	1	2	3	4	5	6	7	8	9	10	11	12	13	14	15
Preadjustment	25	37	30	28	33	30	50	50	35	40	42	110	55	34	33
Postadjustment	N/A	N/A	N/A	N/A	N/A	N/A	30	30	N/A	32	30	29	23	29	25

5. Future

For the 10 m antennas, there is some indication of the need for small panel adjustment. We await the optimization of the receiver biasing, tuning and possibly bandpass before proceeding with slightly higher resolutions maps, mostly to verify the orientation of the maps before proceeding with adjustment. While the tuning to frequency with a better system temperature for the 10 m antennas is now possible the other improvements are not yet available. If this new data shows a need to adjust panels or provides further insight into the residual illumination misalignment we may choose to perform further adjustment.

For the 6 m antennas, the situation is more complicated. To provide resolution on the mounting screw scale, we must have aperture surface images with a resolution of ~ 10 cm. While such resolution is not possible on astronomical sources, we can obtain the necessary signal to noise using a narrow band transmitter. The transmitter has recently been moved to a distance near the near-field limit of the 6 m antennas. It is, however, not visible to C9 and C13. Holography on the remaining 6 m antennas can be done at the same time using C6 for a reference antenna while C3, the other 10 m antenna which has a clear line of sight to the transmitter, cannot be used as it has no receiver. As a complication, the transmitter is at a low elevation angle and the amount of verticle resolution which can be achieved is small. There is some concern that reflections may limit the utility of the transmitter, but this remains to be verified. Ultimately, to utilize the high signal to noise of the transmitter on a time scale in which we need not also consider changes in atmospheric conditions, we require on-the-fly mapping capabilities. Current methods of individual pointings would require so long to complete that we would have to contend with illumination effects from the sun. Further adjustment of the 6 m antenna will likely await these improvements.

6. Acknowledgements

10 m alignment: Dave Woody performed the optical alignment. Stan Hudson constructed the tool necessary to do the alignment.

6 m adjustment: Dick Plambeck provided overlays of screw positions and created maps with screw turns in degrees instead of the maps shown here. Dustin Madison, Douglas Bock, Andrew West, and Dick Plambeck helped with panel adjustments.

7. References

Cornwell, T.J., Holdaway, M.A. & Uson, J.M., 1993, *A&A* 271, 697.

Sault, R. J., Teuben, P. J. & Wright, M. C. H., 1995, *ASP Conf. Ser. 77: Astronomical Data Analysis Software and Systems IV*, ed. Shaw, R. .A., Payne, H. E. & Hayes, J. J. E., 433